Salt Effects on the Structure and Internal Dynamics of Superhelical DNAs Studied by Light Scattering and Brownian Dynamics

Markus Hammermann,* Carola Steinmaier,# Holger Merlitz,§ Ulrike Kapp,¶ Waldemar Waldeck,* Giuseppe Chirico,‖ and Jörg Langowski*

*Division of Biophysics of Macromolecules, German Cancer Research Center, D-69120 Heidelberg, Germany; #SAP AG, D-69190 Walldorf, Germany; §Max-Planck-Institut für Kernphysik, D-69029 Heidelberg, Germany; ¶EMBL, Grenoble Outstation, F-38042 Grenoble Cedex, France; and ‖I.N.F.M. Dipartimento di Fisica, Università degli Studi di Milano, I-20133 Milano, Italy

ABSTRACT Using laser light scattering, we have measured the static and dynamic structure factor of two different superhelical DNAs, p1868 (1868 bp) and simian virus 40 (SV40) (5243 bp), in dilute aqueous solution at salt concentrations between 1 mM and 3 M NaCl. For both DNA molecules, Brownian dynamics (BD) simulations were also performed, using a previously described model. A Fourier mode decomposition procedure was used to compute theoretical light scattering autocorrelation functions (ACFs) from the BD trajectories. Both measured and computed autocorrelation functions were then subjected to the same multiexponential decomposition procedure. Simulated and measured relaxation times as a function of scattering angle were in very good agreement. Similarly, computed and measured static structure factors and radii of gyration agreed within experimental error. One main result of this study is that the amplitudes of the fast-relaxing component in the ACF show a peak at 1 M salt concentration. This nonmonotonic behavior might be caused by an initial increase in the amplitudes of internal motions due to diminishing long-range electrostatic repulsions, followed by a decrease at higher salt concentration due to a compaction of the structure.

INTRODUCTION

The three-dimensional folding of DNA in the cell is a determining factor in processes in the cell cycle such as mitosis, transcription, replication, and recombination. Although the compaction of DNA is mainly due to interaction with proteins such as histones, internal elastic strain of the DNA chain is of great importance for determining intramolecular interactions and the association of regulatory proteins with the DNA (Langowski, 1997). Torsional stress in the DNA chain, generated, e.g., during the course of transcription, causes the folding of DNA into a superhelix. In that structure, intramolecular interactions differ from those in an unstressed wormlike coil; evidence for this is given by supercoiling-induced DNA looping (Borowiec et al., 1987) and by recent model calculations (Klenin et al., 1995; Vologodskii et al., 1992). It has also been reported that local DNA structural transitions, such as sequence- or protein-induced curvature, could control the global structure of the superhelix and therefore modulate interactions between distant sites (Klenin et al., 1995; Kremer et al., 1993; Laundon and Griffith, 1988; ten Heggeler-Bordier et al., 1992; Zhang et al., 1994).

Understanding the many facets of supercoiling in the biological functions of DNA requires a detailed understanding of the structure of superhelical DNA under conditions similar to those in living cells. DNA several kilobases in length is a highly flexible molecule which at room temperature cannot be described by any single equilibrium structure. Its thermodynamic equilibrium state is best described by an ensemble of molecules of widely varying conformation, which all have approximately the same internal energy (Langowski et al., 1996). Thus, resolving its structure at atomic detail is neither possible nor desirable. To assess the equilibrium conformation of superhelical DNA, one must rather resort to methods that yield information about average structural and dynamic properties of the molecule free in solution, such as radius of gyration, diffusion coefficients, or parameters related to internal bending and twisting motion, and their dependence on external parameters like salt concentration or superhelix density. Suitable models have then to be used that relate those solution properties to underlying physical properties of the DNA chain, like bending, twisting, and stretching elasticity; DNA radius; and electrostatic interactions.

Recently, attention has focused on the interaction between opposing double strands in an interwound superhelix and its modulation by the concentration of counterions. Specifically, Bednar et al. (1994) observed in cryoelectron microscopy studies a lateral collapse of the interwound structure for Na^+ concentrations greater than 0.1 M or at millimolar concentrations of Mg^{2+}. The relevance of this observation for the solution structure of the superhelix has been called into question by recent results of Gebe et al. (1996), who could not find evidence for such a collapse in static and dynamic light scattering (SDLS), fluorescence polarization anisotropy decay (FPA), or circular dichroism (CD) measurements.

Whereas these and other studies emphasize the importance of electrostatic interactions in understanding the struc-

Received for publication 19 December 1996 and in final form 24 July 1997.

Address reprint requests to Dr. Jörg Langowski, Deutsches Krebsforschungszentrum, Abteilung Biophysik der Makromolekule (0830), Postfach 101949, D-69009 Deidelberg, Germany. Tel.: 49-6221-423390; Fax: 49-6221-423391; E-mail: joerg.langowski@dkfz-heidelberg.de.

0006-3495/97/11/2674/14 $2.00

ture of superhelical DNA, the dependence of its structure and dynamics on salt concentration has not been explored very systematically so far. It has been shown by dynamic light scattering (DLS) measurements that the internal motions of superhelical DNA increase with salt concentration (Langowski, 1987), but for lack of a suitable model, this effect could only be interpreted qualitatively. Here we have studied the dependence of the radius of gyration and the dynamic structure factor of two superhelical DNAs of different sizes in the range of 1 mM to 3 M Na^+ concentration. We compare the experimental data with predictions from a recently proposed Brownian dynamics (BD) model that has been shown to successfully describe the equilibrium structural properties of superhelical DNA and the dynamics of superhelix formation (Chirico and Langowski, 1992, 1994, 1996).

MATERIALS AND METHODS

Construction of p1868

One of the aims of this study was to measure dynamic light scattering data on a superhelical DNA as small as possible. This has several advantages: the numerical simulation of trajectories of smaller DNAs is much less expensive in terms of CPU time, the equilibrium structure is straight interwound without branches, and the DNA can be separated into much narrower topoisomer fractions by high-performance liquid chromatography. We therefore constructed a derivative of pUC18 by deleting the polylinker region, the *lacZ'* gene, and as much of the remaining sequence as possible, so that a functional origin of replication and the ampicillin resistance marker were still present. The deleted region of pUC18 and the map of the resulting plasmid, p1868 (1868 bp), are shown in Fig. 1. In 10-liter fermenter cultures with LB medium containing 100 μg/ml ampicillin, and after overnight amplification with 150 μg/ml chloramphenicol at a cell density of OD_{600} = 1.0, the yield of pure superhelical DNA is ~2 mg/liter of culture, comparable to that of pUC18.

Superhelical DNA preparation

pUC18 plasmid DNA was prepared from *Escherichia coli* HB 101 as described (Kapp and Langowski, 1992; Langowski, 1987); p1868 was then constructed as described above. SV40 viral DNA was prepared from infected CV1 monolayer cells according to the method of Waldeck et al. (1988). After ethanol precipitation and a short drying time, the DNA was in both cases dissolved in TE buffer (10 mM Tris-HCl, pH 7.5, 1 mM EDTA). For additional purification and concentration, the DNA was precipitated for 15 h on ice by adding a 30% stock solution of polyethyleneglycol (PEG) 6000 in 1.6 M NaCl to a final PEG concentration of 8.6% in 0.46 M NaCl for SV40 DNA and by adding a 50% solution of PEG 20000 in 0.5 M NaCl to a final PEG concentration of 10% in 0.6 M NaCl for p1868, respectively. The DNA was pelleted at 8000 rpm and 4°C in the HB4 rotor in a Sorvall RC-5B centrifuge and again dissolved in TE buffer. Supercoiled and relaxed plasmids were separated by high-performance liquid chromatography, as described by Kapp and Langowski (1992). The integrity of the DNA plasmids and the superhelical density were controlled by agarose gel electrophoresis (1%) in Tris-acetate buffer (40 mM Tris-acetate, 2 mM EDTA, pH 8). Only samples containing more than 90% supercoiled DNA were used for DLS measurements in two different buffers: 5 mM Na-phosphate, 1 mM EDTA, pH 8.0 (buffer I), and 10 mM Na-cacodylic acid, 1 mM EDTA, pH 7.0 (buffer II). The NaCl concentration was varied between 1 and 3000 mM and controlled by conductivity measurements. DNA concentrations were always 25–50 μg/ml.

Light scattering measurements

p1868 plasmids were filtered slowly (1–2 ml/min) through 0.1-μm polycarbonate membrane filters (Nuclepore, Pleasanton, CA), SV40 DNA was filtered through 0.2-μm and 0.4-μm membrane filters (Whatman, Maidstone, England) into a cylindrical quartz scattering cell of 1 cm diameter

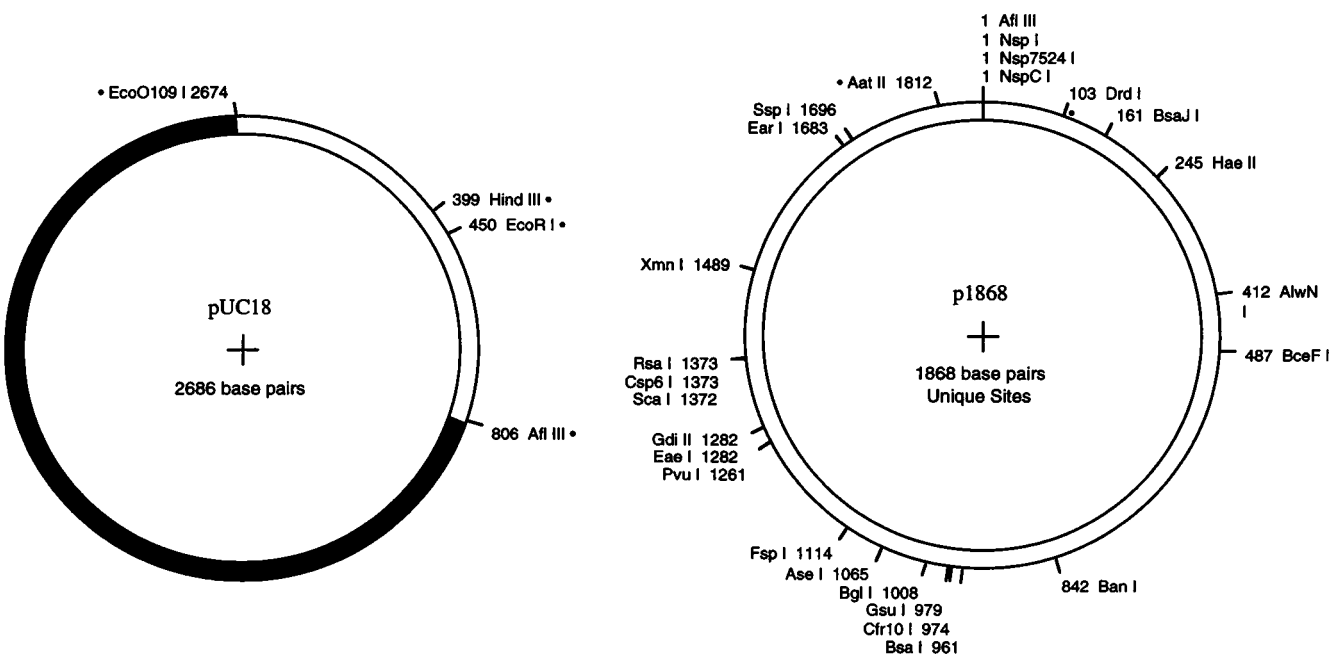

FIGURE 1 Construction of p1868. (*Left*) Deleted region of pUC18 (*white*). (*Right*) Map of p1868 DNA.

(Hellma, Mülheim, Germany), which had been rinsed with at least 10 ml of filtered buffer I or buffer II before use.

Light scattering measurements were performed with vertically polarized argon laser light at 488 nm (Spectra-Physics 2020). The typical power used was 500 mW in TEM_{00}. The sample cuvette was in the center of a cylindrical index matching bath filled with water of 20°C. The scattered light was detected by a photomultiplier (Thorn EMI PM28B for p1868, ALV SO-SIPD Dual (Langen, Germany) for SV40 DNA) on an ALV goniometer arm. The correlator was a 288-channel ALV-5000 multiple tau digital correlator (Langen, Germany).

After careful filtering, dust particles were observed only occasionally (about once every 10 s) over the length of the laser beam traversing the scattering cell. The length of the observed scattering volume was ~200 μm; hence the probability of a dust particle entering this volume was on the order of once every few minutes. Stray dust events were completely eliminated by a "software dust filter," which collected the data in batches and rejected any data where dust contamination was suspected (see below).

The static light scattering measurements yielded the angle-dependent Rayleigh ratio

$$R_R(\theta) = \frac{I_S(\theta)}{I_0} r^2 = K_o c M P(\theta) \tag{1}$$

where $I_s(\theta)$ is the scattering intensity as measured by the photomultiplier, I_0 is the intensity of the incident light as measured by a photodiode, r is the distance between the scattering volume and the detector, θ is the scattering angle, c is the concentration, M is the molecular weight of the molecules, $P(\theta)$ is the form factor, and K_0 is an optical constant. To calibrate the instrument, a standard measurement was made with toluene; we used a standard Rayleigh ratio of 2.942×10^{-5} cm^{-1} at 25°C, as given by ALV (Langen).

For dynamic light scattering, autocorrelation functions (ACFs) were collected in batches of 10 s. Batches in which intensity peaks occurred that exceeded the mean by more than 30 standard deviations were discarded because of dust contamination. The accumulation was continued for a total of 1000 s per angle (100 "good" batches). To resolve the components in the ACF, two different programs were used: PCSFIT fits a squared sum of exponentials to the ACF (Langowski and Giesen, 1989). MEXDLS (Langowski and Bryan, 1991) is based on a maximum entropy procedure; the program fits a distribution of exponentials to the ACF. It has been shown that the resolution of MEXDLS determining components in a measured ACF is comparable to or even better than the resolution of CONTIN (Provencher, 1984); diffusion coefficients separated by a factor of 3 can be resolved (Langowski and Bryan, 1991).

DNA simulations

The dynamics of p1868 and SV40 DNA were simulated by the use of a Brownian dynamics (BD) algorithm described elsewhere (Chirico and Langowski, 1992, 1994; Langowski et al., 1994a). The DNA was modeled as a flexible polymer and divided into 50 (p1868) and 140 (SV40) segments of 12.6-nm length corresponding to 37.4 bp. Because this is significantly smaller than the persistence length (assumed here 50 nm), the individual segments can be regarded as rigid rods. The torsional rigidity was set to $C = 2.6 \times 10^{-19}$ erg-cm, as in previous publications (Chirico and Langowski, 1992, 1994).

The electrostatic forces in the model were described as Debye-Hückel interactions between cylindrical DNA segments. using a procedure similar to that described by Chirico and Langowski (1996). The starting point was the expression for the electrostatic energy of interaction between two uniformly charged nonadjacent segments i, j in the Debye-Hückel approximation

$$\frac{E_{ij}}{k_B T} = \frac{\nu^2}{k_B T D} \int d\lambda_i \int d\lambda_j \frac{e^{-\kappa r_{ij}}}{r_{ij}}. \tag{2}$$

The integration is done along the segments, λ_i and λ_j are the distances from the segment beginnings, r_{ij} is the distance between the current positions at the segments to which the integration parameters λ_i and λ_j correspond, and κ is the inverse of the Debye length, so that

$$\kappa^2 = \frac{8\pi e^2 I}{k_B T D}. \tag{3}$$

I is the ionic strength, e is the proton charge, D is the dielectric constant of water, and ν is the linear charge density, which is equal to $-2e/\Delta$ for DNA, where Δ is the distance between the base pairs. The linear charge density was renormalized to take into account the immobile counterions and the excluded volume effects (Stigter, 1977).

The forces were parameterized by using the distance between the DNA segments and three angles describing their relative orientation. At the beginning of the simulation, a table containing these forces was precalculated, and during the simulations the electrostatic forces could be obtained by a simple table lookup. A detailed description of this method will be given in a forthcoming publication (Klenin et al., manuscript in preparation).

The deficit linking number in the simulations was set to the native value measured for each plasmid in gel electrophoresis buffer, $\Delta Lk = -10$ for p1868 and $\Delta Lk = -24$ for SV40, corresponding to superhelical densities of $\sigma = -0.056$ (p1868) and -0.048 (SV40). These values were not varied for the simulations at different ionic strengths. This was not considered a critical restriction in the calculations for the following reason: the salt-induced change in superhelical density as measured by Anderson and Bauer (1978) is $d\sigma/d \log[Na^+] = -0.0045$. The total variation in σ is therefore -0.009 from 0.01 M to 1 M Na^+; because the ionic strength of the electrophoresis buffer, where σ was measured, was 40 mM, this leads to a variation in superhelical density from -0.053 to -0.062 for p1868 and -0.045 to -0.054 for SV40 in the measurements. In another set of measurements (Richter, 1997), we found no major change in radius of gyration for superhelical DNAs in this range of superhelical densities.

Simulations were performed either with a time step $\delta t = 1$ ns and a stretching elastic potential corresponding to a bond length variance $\delta = 0.08$, or with $\delta t = 0.1$ ns and $\delta = 0.008$. All simulations were carried out assuming water viscosity and a temperature of $T = 20°$, starting from a flat circle as initial configuration. The trajectories of the DNA plasmids were computed for a total time of 1 ms. Both the writhe and the radius of gyration of the configuration had reached equilibrium after ~500 μs for the longest DNA (SV40); for calculating static and dynamic structural quantities, we took an average over the last 500 μs of the trajectory. Detailed investigations on the dependence of the characteristic time to reach equilibrium on DNA length will be published elsewhere (Wedemann et al., manuscript in preparation). A simulation time of 100 μs on the SV40-DNA circle with $\delta = 0.008$ and $\delta t = 0.1$ ns took ~500 h CPU time on a SG Indigo 4400 and about half that time on an IBM SP2.

The radius of gyration of the simulated plasmids could be calculated directly from the trajectory during the simulation:

$$R_g = \frac{1}{2N^2} \sum_{i=1}^{N} \sum_{j=1}^{N} (\mathbf{r}_i - \mathbf{r}_j)^2 \tag{4}$$

where N is the number of segments and $\mathbf{r}_i$ and $\mathbf{r}_j$ are the positions of the segments i and j. The form factor $P(\mathbf{q})$ could also be calculated from the trajectory,

$$P(\mathbf{q}) = \frac{1}{N^2} \sum_{i=1}^{N} \sum_{j=1}^{N} \frac{\sin(\mathbf{q}(\mathbf{r}_i - \mathbf{r}_j))}{\mathbf{q}(\mathbf{r}_i - \mathbf{r}_j)} \tag{5}$$

where q is the scattering vector:

$$q = \frac{4\pi n}{\lambda} \sin\left(\frac{\theta}{2}\right) \tag{6}$$

n is the refractive index of the solvent, λ is the wavelength, and θ is the scattering angle.

To quantify the superhelix diameter, we calculated the average distance between each DNA segment i and its nearest neighbor j, while skipping the five nearest neighbors along the DNA strand:

$$D_{\text{superhelix}} = \langle|\vec{r}_i - \vec{r}_j|\rangle. \tag{7}$$

The dynamic structure factor $S(q, \tau)$ could be calculated from the trajectory, assuming segments of equal and isotropic scattering power:

$$S(\mathbf{q}, \tau) = \frac{1}{N^2}\left\langle \sum_{i=1}^{N}\sum_{j=1}^{N} e^{i\mathbf{q}(\mathbf{r}_i(t)-\mathbf{r}_j(t+\tau))}\right\rangle_t \tag{8}$$

where $\langle\ \rangle_t$ indicates the time average. This quantity is directly related to the scattered light-intensity autocorrelation function:

$$G_2(\mathbf{q}, \tau) = \frac{\langle I(\mathbf{q}, \tau), I(\mathbf{q}, 0)\rangle}{\langle I(\mathbf{q}, 0)\rangle^2} = 1 + \left[\frac{S(\mathbf{q}, \tau)}{S(\mathbf{q}, 0)}\right]^2 \tag{9}$$

To compare the full course of the measured ACF with the simulation, it would be necessary to compute the theoretical ACF out to approximately two or three translational relaxation times, corresponding to several milliseconds. To obtain sufficient statistical accuracy, trajectory lengths of 10–100 ms would then be necessary, which are beyond the limits of most present-day machines.

However, the slowest fluctuations in the computed ACF arise through the center of mass diffusion of the molecule. Shorter trajectories might be sufficient to calculate at least the internal relaxation times if one could separate the center of mass diffusion contributions from those due to internal motions. One approximative way of separating the Brownian motion of a circular semiflexible chain into a number of "modes" has been presented by Berg (1979), and later in a modified way by Soda (1984). Although the Berg-Soda (BS) model describes the dynamics of a real wormlike chain only approximately—the longitudinal elasticity of the chain is assumed to be directly related to the bending persistence length, and torsional forces are neglected—we use it here simply as a method for decomposing the correct ACF computed from the simulated trajectory into a set of suitable relaxation modes. These functions are not "normal modes" in the strict sense but represent a set of approximate coordinates that can be useful for describing the dynamics of the system. We expect that any difference in the dynamic behavior between the BS model and a real superhelical DNA is contained in the amplitudes and relaxation times characterizing these modes, which are obtained from a fit to the (noisy) simulation data. Therefore, when we reconstruct a smoothed version of the ACF from these modes, we can expect it to be a valid approximation of the ACF that would be obtained by direct computation from a much larger trajectory.

In the BS model, the segment positions $\mathbf{r}_j(t)$ of a relaxed circular semiflexible chain in the laboratory frame (i.e., frame origin fixed in space) are expressed as an expansion in Fourier coordinates $\mathbf{b}_n(t)$:

$$\mathbf{r}_j(t) = \frac{1}{\sqrt{N}}\sum_{n=1}^{N} \mathbf{b}_n(t)e^{i2\pi nj/N} \tag{10}$$

or

$$\mathbf{b}_n(t) = \frac{1}{\sqrt{N}}\sum_{j=1}^{N} \mathbf{r}_j(t)e^{-i2\pi jn/N}$$

The time correlation functions of the Fourier coordinates are single exponential decays:

$$c_n(t) = \langle \mathbf{b}_n(t)\cdot\mathbf{b}_n(0)\rangle = \langle|\mathbf{b}_n(0)|^2\rangle e^{-t/\tau_n} \tag{11}$$

with amplitude $\langle|\mathbf{b}_n(0)|^2\rangle$ and relaxation time τ_n characterized by the elastic and frictional properties of the chain (Soda, 1984). Soda's approximate analytical result for the dynamic structure factor of a circular chain is then

$$S(\mathbf{q}, \tau) = \exp(-D_{cm}\mathbf{q}^2\tau) \cdot \sum_{j,k=1}^{N} \exp\left\{-\frac{\mathbf{q}^2}{3N}\sum_n\left[c_n(0) - c_n(\tau)\cos\left(\frac{2\pi}{N}(j-k)\tau\right)\right]\right\} \tag{12}$$

where D_{cm} is the center-of-mass diffusion coefficient of the chain.

Our assumption is now that this Fourier decomposition can also be applied to trajectories arising from related systems, namely circular wormlike chains with topological constraint, and that the $c_n(t)$ can still be approximated by single exponential decays, albeit with different amplitudes and relaxation times.

Fig. 2 shows that the amplitudes $\langle|\mathbf{b}_n(0)|^2\rangle$ and relaxation times τ_n indeed differ between the BS model and a Brownian dynamics simulation of a superhelical DNA. The values of τ_n as obtained from the BS model (equation 53 in Soda, 1984) plotted against $\langle|\mathbf{b}_n(0)|^2\rangle$ (equations 34 and 36 of Soda) follow a power law with exponent 1.8 (Fig. 2, *solid line*). The corresponding quantities from the BD simulation computed through a single-exponential fit to Eq. 11 with the correlation functions computed from a simulated trajectory of superhelical SV40-DNA also follow a power law for the lower-order modes, but with exponent 1.3 ± 0.25. For the high-frequency modes, the simulated data approach the curve from the Soda model.

Our procedure allowed us to calculate the approximative contribution of the center-of-mass diffusion and the internal motions to the dynamic structure factor. First the center-of-mass contribution was separated from the internal motion by calculating the diffusion coefficient D_{cm} from the simulated trajectory by a linear fit to a plot of $|\mathbf{r}_{cm}(t) - \mathbf{r}_{cm}(0)|^2$ versus t. Equation 8 was then rewritten in the form

$$S(\mathbf{q}, \tau) = \exp(-D_{cm}\mathbf{q}^2\tau)\frac{1}{N^2} \cdot \left\langle \sum_{i=1}^{N}\sum_{j=1}^{N} \exp[i\mathbf{q}(\rho_i(t) - \rho_j(t+\tau))]\right\rangle_t \tag{13}$$

where $\rho_i(t) = \mathbf{r}_i(t) - r_{cm}(t)$. This decomposition is based on the assumption of a loose correlation between the center of mass and the internal motions.

The bead positions, expressed in the laboratory frame, satisfy the relation $\mathbf{r}_{k+N}(t) = \mathbf{r}_k(t)$ and are transformed into Fourier coordinates by Eq. 10. To follow the treatment given by Soda (1984), one must now ensure that

$$\langle \mathbf{b}_n(t)\cdot\mathbf{b}_m(t)\rangle \ll \langle \mathbf{b}_n^2(t)\rangle, \langle \mathbf{b}_m^2(t)\rangle \tag{14}$$

for $n \neq m$, which is approximately the case for our simulations (see Fig. 3). The small residual correlation between the first and the higher modes can be empirically described by an exponential law of the type $\langle \mathbf{b}_1(t)\cdot\mathbf{b}_m(t)\rangle \cong \langle \mathbf{b}_1(t)\cdot\mathbf{b}_1(t)\rangle \cdot 0.07e^{-0.35(m-1)}$, and its contribution to the first mode correlation function amounts to 10–15%.

Furthermore, in the BS model, the $\mathbf{b}_n(t)$ are linearly independent Gaussian-distributed random variables with zero mean. The Fourier coordinates $\mathbf{b}_n(t)$ computed on the simulated trajectories also obeyed a Gaussian distribution, as shown in Fig. 4. The $\mathbf{r}$ coordinates will fluctuate around their initial positions, $\langle \mathbf{r}_n(t)\rangle = \mathbf{r}_n(0)$; thus they will not have exactly zero mean in general. But because their variance increases with time and their mean stays constant, for long times $|\langle \mathbf{r}_n(t)\rangle|^2 \ll \langle|\mathbf{r}_n(t)|^2\rangle$, linear combinations of the $\mathbf{r}_n$, such as the $\mathbf{b}_n(t)$, should also have $|\langle \mathbf{b}_n(t)\rangle|^2 \ll \langle|\mathbf{b}_n(t)|^2\rangle$. This is approximately fulfilled for the higher modes; the lowest mode and the center-of-mass position had mean values significantly different from zero because of the statistics of the present simulations. We can estimate

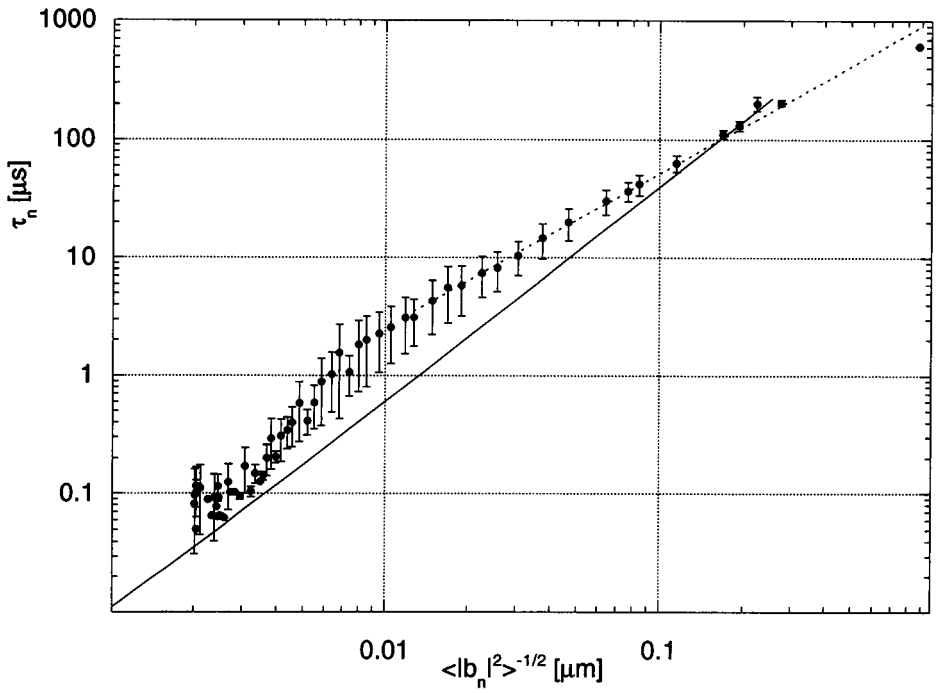

FIGURE 2 Relationship between the mode amplitudes $\langle b_n^2 \rangle$ and the relaxation times τ_n for the BS model on a 5243-bp circular DNA (——), and a 500-μs trajectory of a BD simulation of superhelical SV40-DNA (●, 1σ error bars). - - - -, Power law fit to the upper part of the BD data, exponent 1.3 ± 0.25.

the error introduced by the nonadequate statistics by using the relation (Doi and Edwards, 1986, Appendix 2.I, p. 35)

$$\langle \exp(i\mathbf{q}\cdot\mathbf{b}_n)\rangle = \exp(i\mathbf{q}\langle\mathbf{b}_n\rangle)\exp\left(-\frac{\mathbf{q}^2\cdot(\langle|\mathbf{b}_n|^2\rangle - |\langle\mathbf{b}_n\rangle|^2)}{2}\right) \quad (15)$$

from which we find that after averaging over all orientations of q, the nonvanishing mean of b_1 changes the relaxation amplitude of the first Fourier mode by a factor of approximately $\sin(|\mathbf{q}||\langle\mathbf{b}_1\rangle|)/(|\mathbf{q}||\langle\mathbf{b}_1\rangle|)\exp(|\mathbf{q}|^2|\langle\mathbf{b}_1\rangle|^2/2)$. However, this does not lead to a significant change in the relaxation rates as compared to a very long trajectory. Because the lowest order mode contributes most to the dynamic structure factor, this deviation might have resulted in some overestimate of the amplitude of the internal motion part of the structure factor, but only slightly affected the relaxation times. For the higher Fourier modes, the corrections are much smaller, because Eq. 14 is very well satisfied in these cases.

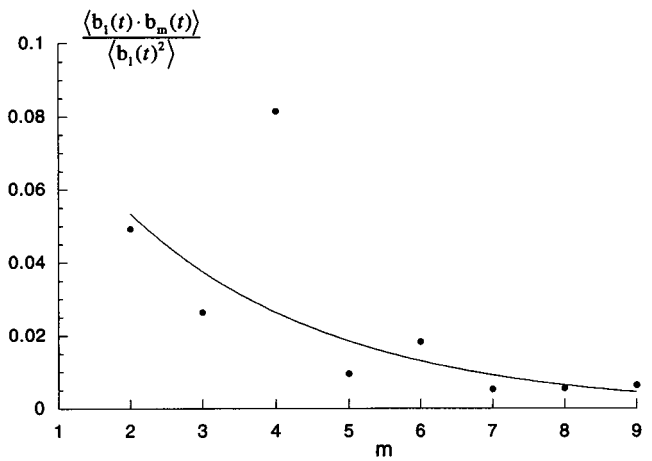

FIGURE 3 $\langle \mathbf{b}_1(t)\cdot\mathbf{b}_m(t)\rangle/\langle \mathbf{b}_1(t)^2\rangle$ versus m for SV40 at 100 mM NaCl concentration, averaged over the relaxed part of the trajectory (last 500 μs). The decrease in amplitude of the cross-correlation between the modes can be fitted empirically to an exponential decay, $\langle \mathbf{b}_1(t)\cdot\mathbf{b}_m(t)\rangle \cdot \langle \mathbf{b}_1(t)\cdot\mathbf{b}_1(t)\rangle \cdot 0.07e^{-0.35(m-1)}$ for $m > 1$.

The raw correlation functions $c_n(t)$ were calculated by using Eq. 11. Single exponential decays were fitted to the correlation functions by a nonlinear least-squares procedure, yielding $c_n(0)$ and τ_n. The range of the τ_n was from ~60 ns to 600 μs.

The dynamic structure factor could be reconstructed from these quantities and the center-of-mass diffusion coefficient by Eq. 12. The normalized structure factor yielded a theoretical autocorrelation function (Eq. 9), which could be analyzed by using the same fitting procedures as for the measured ACFs.

Our approach is essentially a Fourier smoothing procedure, where the dynamics of the system are separated into a convenient set of coordinates from which the dynamic structure factor can be reconstituted. It should be in first approximation insensitive to the underlying physics of the chain, i.e., local variations of the DNA structure or potentials between segments. The tests shown in Figs. 2–4 ensure that the procedure applied here to BD trajectories of superhelical DNA is approximately valid. The quality of this approximation will probably depend on the chain geometry, and in the absence of a formal proof that the decomposition of the dynamic structure factor is complete, one should check the linear independence of the modes and the Gaussian zero mean distribution of the bead positions before applying the method to other systems. For other DNAs and wormlike chain polymers with similar underlying physics (e.g., stiff polysaccharide), the limits of the procedure should be very similar. The method might not be applicable, however, to analyzing the dynamic structure factor of rigid objects with strong internal interference. Gebe and Schurr, for example, calculated oscillations in the dynamic structure factor of rigid rings (Gebe and Schurr, 1993), and these cannot occur in Eq. 10, which decays monotonically with increasing $\mathbf{q}$.

RESULTS AND DISCUSSION

Static light scattering

We found that the static structure factor $P(q)$ of superhelical DNA can be well approximated by that of a Gaussian

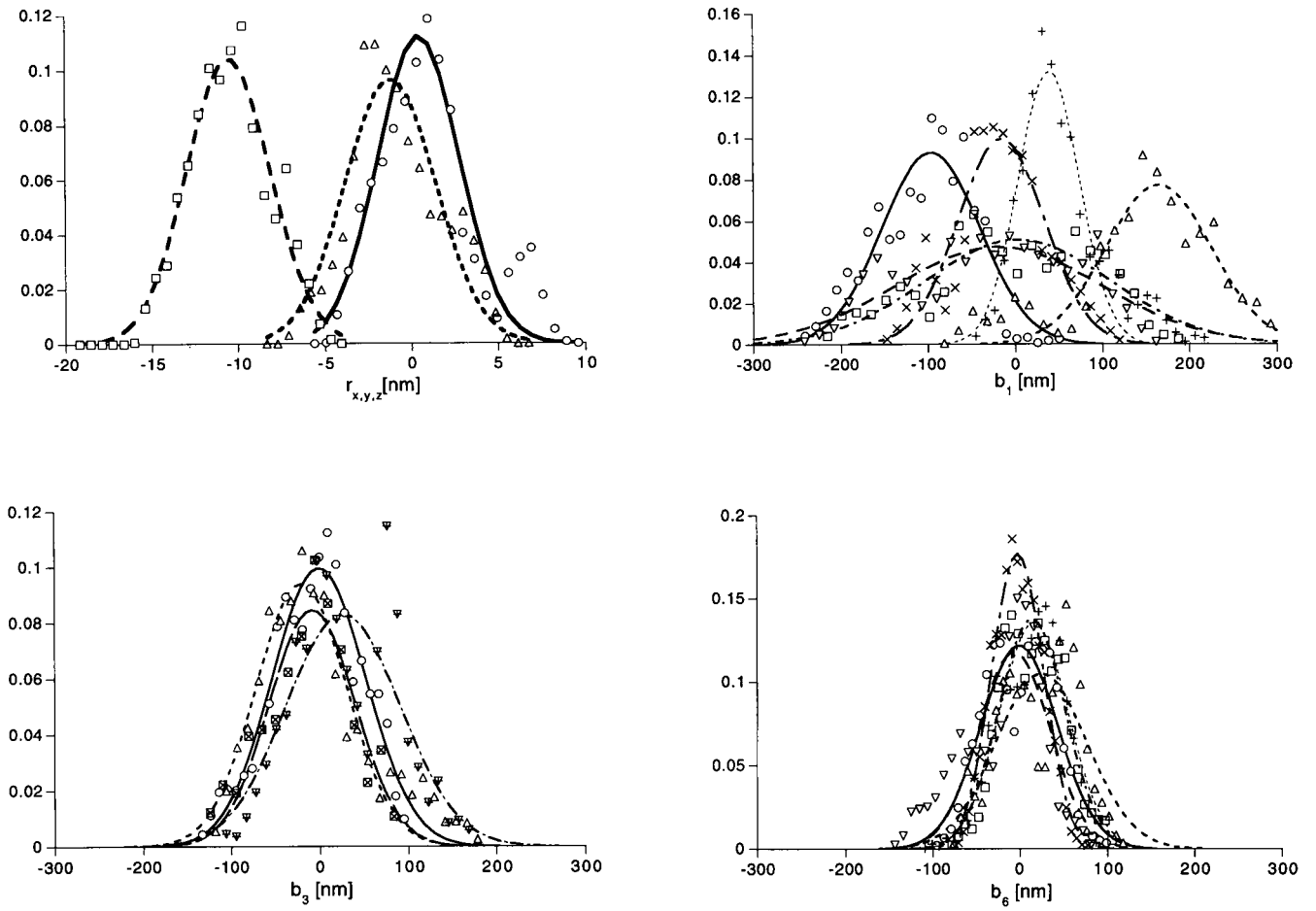

FIGURE 4 Distribution of the x, y, and z components of bead no. 10 $\mathbf{r}_{10}(t)$, and real and imaginary x, y, and z components of the Fourier coordinates $\mathbf{b}_n(t)$ for $n = 1, 3, 6$ from the relaxed part of the trajectory. ○, △, □, Real x, y, and z components. ▽, ×, +, Imaginary x, y, and z components. The curves shown are Gaussian distributions fitted to the data points.

random coil,

$$P(q) = \frac{2}{a^2}[\exp(-a) + a - 1]; \quad a = \frac{q^2\langle D^2\rangle}{6} \qquad (16)$$

where $\langle D^2\rangle$ is the average squared end-to-end distance of the coil, related to the radius of gyration:

$$R_G = \sqrt{\frac{\langle D^2\rangle}{6}} \qquad (17)$$

Fig. 5 shows the superposition of the measured structure factor of SV40 DNA and the theoretical structure factor of a random coil (Eq. 16). Apparent radii of gyration were evaluated by fitting Eq. 16 to the measured data. The dependence of the radius of gyration on the Na^+ concentration is shown for the two plasmids in Fig. 6. The radius of gyration decreases with salt concentration for both DNAs; this decrease becomes more pronounced above 1.0 M NaCl for SV40 DNA. This indicates a compaction of the whole superhelix structure due to screening of the negatively charged DNA backbone by the Na^+ counterions.

If one regards the plectonemic superhelix as a wormlike polymer whose contour is given by the superhelix axis, one may estimate a "persistence length" for this chain from the measured end-to-end-distances $\langle D^2\rangle$ of the Gaussian coil fit (Eq. 17).

The relationship between $\langle D^2\rangle$ and the persistence length L_p is given by the Porod-Kratky equation (Kratky and Porod, 1949):

$$\langle D^2\rangle = 2L_pL_c\left[1 - \frac{L_p}{L_c}(1 - e^{-L_c/L_p})\right] \qquad (18)$$

We found L_p = 25 nm for SV40 DNA (<1 M NaCl) and L_p = 40 nm (0.1 M NaCl) to 45 nm (0.01 M NaCl) for p1868 DNA. Thus the superhelix axis has an apparent persistence length that is even smaller than the 50 nm characterizing linear B-DNA (Hagerman, 1988). This result is implausible because one should suppose that a superhelix made of two interwound double helices is stiffer than a single stretch of B-DNA. The discrepancy between the estimated persistence lengths for the superhelix axis and the reported value for linear DNA is greater for the longer DNA.

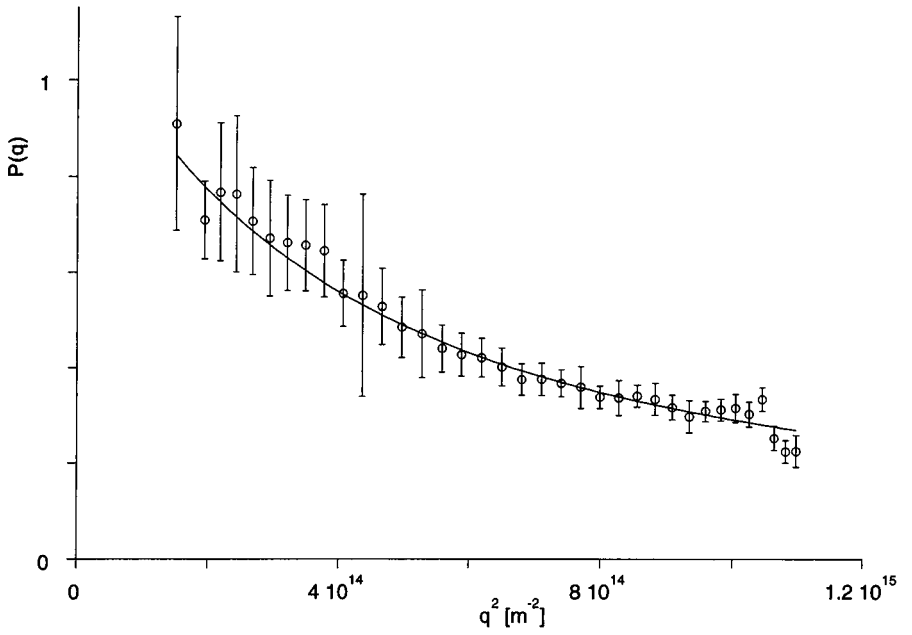

FIGURE 5 Light scattering structure factor of SV40-DNA at 0.1 M NaCl as a function of the square of the scattering vector. The data were fitted using the theoretical structure factor of a random coil (Eq. 16).

An explanation of this result might be branching of the superhelix. At equal stiffness, a branched polymer will be more compact than a linear chain of the same molecular weight; thus the estimated persistence length will be too low in the presence of branches. The branching probability increases with the length of the superhelix; based on the data given by Boles et al. (1990), we estimate very little branching for p1868, whereas most of the molecules of SV40 under these conditions should be branched at least once.

A further indication of DNA branching comes from the comparison of random coil and rigid rod structure factors to the measured static scattering curves: although both DNA molecules show a better fit when the random coil structure factor is used, the p1868 data are closer to the rod structure factor than the SV40 data.

Dynamic light scattering measurements

In earlier work (Langowski and Giesen, 1989; Langowski et al., 1986; Lewis et al., 1985) we and others have shown that the DLS autocorrelation function (ACF) for long DNAs can be described by a bimodal distribution of relaxation components:

$$G^{(2)}(\tau) = 1 + [a_1 e^{-\lambda_1 \tau} + a_2 e^{-\lambda_2 \tau}]^2 \qquad (19)$$

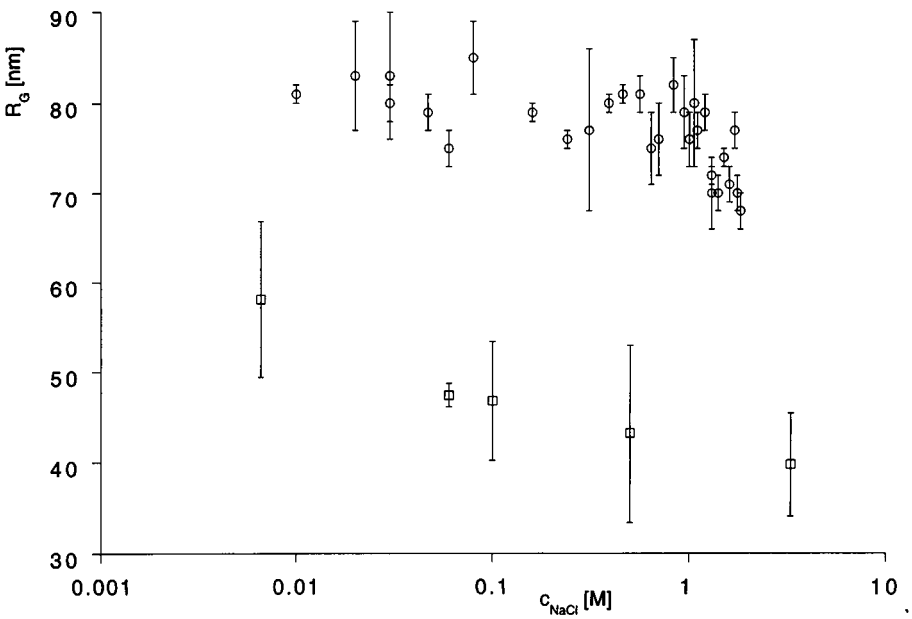

FIGURE 6 Measured radii of gyration of p1868 (□) and SV40 (○) as a function of NaCl concentration.

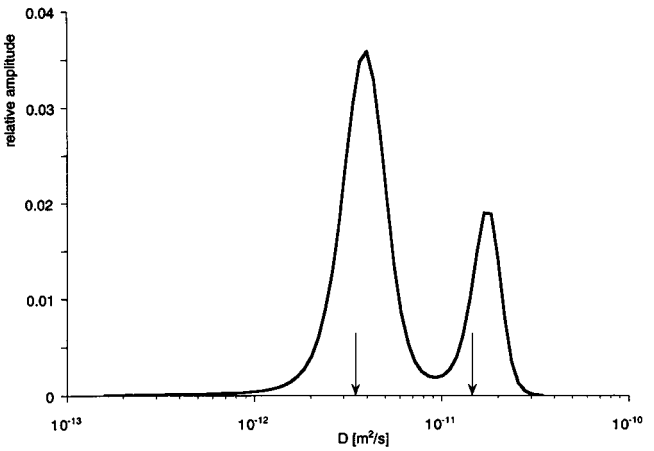

FIGURE 7 Multiexponential distribution computed by MAXENT (*straight line*) compared to discrete exponential fit by PCSFIT (*arrows*) on a DLS autocorrelation function collected for a solution of SV40-DNA at 120° scattering angle. MAXENT yields maxima very close to the discrete diffusion coefficients determined by PCSFIT.

For small scattering vectors $\mathbf{q}$, the slower component λ_1 corresponds to the translational diffusion coefficient D_t: $\lambda_1 = q^2 D_t$, and the faster one, for elongated molecules, is related to the end-over-end rotational diffusion coefficient Θ by $\lambda_2 = 6\Theta + q^2 D_t$. At higher scattering vectors, it has been demonstrated empirically for linear and superhelical DNA that $\lambda_2 = q^2 D_i$, where D_i is an "internal diffusion coefficient" that was interpreted as the relative motion of subsegments of the DNA within the polymer coil (Langowski et al., 1986).

A good estimate of the number of independent relaxation components in the ACF can be obtained through a multiexponential decomposition. This has been done by several groups using programs like CONTIN (Provencher, 1984) or maximum entropy fitting procedures (Gull and Daniell, 1978; Skilling and Bryan, 1984); we used here the latter method, as implemented in our program MEXDLS (Langowski and Bryan, 1991). Here again, we found two main exponential decay components in most of the data sets. A typical diffusion coefficient distribution as computed using MEXDLS is shown in Fig. 7, together with the average diffusion coefficients found by fitting the same ACF to a squared sum of discrete exponentials with the PCSFIT program. The agreement between the two methods is very satisfactory. For the discrete model, we often had to include a third, slow component corresponding to a diffusion coefficient in the range $10^{-13} \ldots 10^{-16}$ m²/s, but whose relative amplitude was always <5%. We attributed this component, which was not considered in further analysis, to residual dust particles that were present in the sample, even after very careful filtering.

In the following, the ACFs were therefore fitted with three discrete exponential components (Fig. 8). As in our earlier studies (Langowski, 1987; Langowski and Giesen, 1989), the translational diffusion coefficient was computed from the main slow relaxation component: $D_t = \lambda_1/q^2$. Although this holds precisely only for $q^2 \rightarrow 0$, we found that D_t did not vary significantly over the whole angular range measured (Fig. 8) and therefore took the average of λ_1/q^2 over all angles as a good estimate for D_t. At high scattering vectors ($q^2 > 6 \times 10^{14}$ m^{-2}) the fast component also increases linearly with q^2 and can therefore be formally interpreted as a diffusion coefficient. It has been shown that for very high scattering vectors the ACF for light scattering from polymers and gels is dominated by the internal diffusion of the smallest independently moving subunit of the molecule (Schurr, 1977); we interpret the λ_2 component as

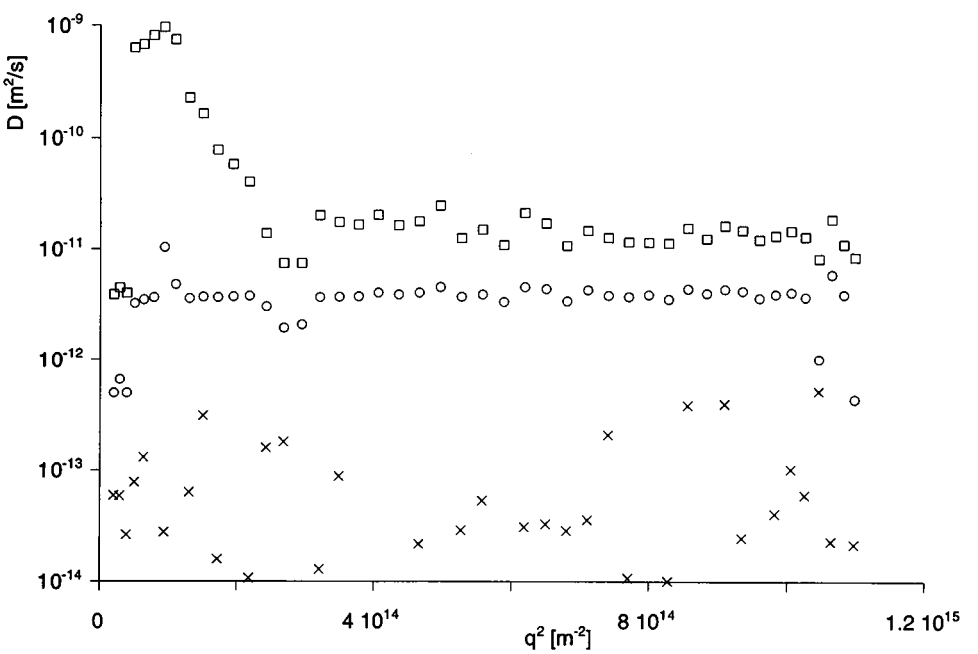

FIGURE 8 Three-exponential fit by PCSFIT to DLS autocorrelation functions collected for a solution of SV40-DNA as a function of the square of the scattering vector. The components were interpreted as translational diffusion coefficient (○), internal diffusion coefficient (□), and a third contribution due to dust particles (×).

TABLE 1 Radii of gyration and diffusion coefficients of the two DNA molecules at 100 mM NaCl as measured by light scattering and as simulated

	p1868	SV40
Experiment		
R_g (nm)	46.8 ± 6.6	80.0 ± 3.0
D_t (10^{-12} m^2s^{-1})	7.0 ± 0.5	3.8 ± 0.4
D_i (10^{-12} m^2s^{-1})	11.0 ± 5.0	13.0 ± 2.0
Simulation		
R_g (nm)	42.6 ± 5.0	74.0 ± 5.0
D_t (10^{-12} m^2s^{-1})	6.6 ± 0.4	4.2 ± 0.3
D_i (10^{-12} m^2s^{-1})	21.0 ± 5.0	17.0 ± 5.0

arising from subunit diffusion within the polymer coil and assign an "internal diffusion coefficient" $D_i = \lambda_2/q^2$. D_t and D_i of p1868 and SV40 (Table 1) are independent of the NaCl concentration, and their dependence on DNA length is in good agreement with previous findings (Langowski and Giesen, 1989). To further quantify the segmental motions, the relative amplitudes $a_2 = A_2/(A_1 + A_2)$ of the fast component were plotted versus q^2. We found an increase in a_2 with q^2, which was shown to be approximately linear for higher scattering vectors ($q^2 > 6 \times 10^{14}$ m^{-2}) (Langowski et al., 1986, 1994b). Because the static structure factor decreases more with the scattering vector for larger particles than for smaller ones, the diffusion of subunits of the DNA chain contributes more to the measured dynamic structure factor at high scattering vectors. Thus a_2 increases with the scattering vector, and the slope m_i of a linear fit of the type $a_2 = m_i \cdot q^2$ for $q^2 > 6 \times 10^{14}$ m^2 can be taken to measure the contribution of the diffusion of subunits to the dynamic structure factor. We interpreted the parameter m_i as a measure of the internal motions and the mobility of subunits of the DNA chain.

Below 1 M NaCl, m_i increases monotonically. At higher salt concentrations m_i decreases again, resulting in a maximum at 1 M NaCl (Fig. 9). The position of this maximum is the same for both DNAs studied; preliminary experiments on the 2686-bp plasmid pUC18 also confirm this peak at the same salt concentration (data not shown).

The salt-dependent variation of m_i reflects a change in the degree of internal motion of the superhelical DNA. In principle, this might be due to either a change of the overall size of the molecule or a change in the internal dynamics of the molecule with unchanged overall shape and dimensions. Here we interpret our data such that over the course of lower salt concentrations, the observed increase in the amplitude of the internal motion parameter is caused by increased screening of the lateral repulsion between neighboring double strands in the plectonemic structure. The scale over which the Debye length changes for monovalent ion concentrations between 10^{-3} and 1 M (10 to 0.3 nm) has to be compared to the expected maximum interstrand separation in an interwound superhelix. Monte Carlo (Klenin et al., 1995) and Brownian dynamics calculations show that this is ~10–15 nm at low ionic strength. The lateral repulsion at low salt in a superhelix is therefore quite significant and might inhibit fluctuations in the superhelix diameter, which at higher ionic strengths will become more pronounced. The decrease in the observed internal motions at NaCl concentrations higher than 1 M, on the other hand, might be due to compaction of the overall DNA structure at high salt, as also indicated by the decrease in the radius of gyration (see Fig. 6).

Another structural transition that has been reported at high salt concentrations is the change to an alternative B′-conformation with a helix pitch of 10.2 instead of 10.4 bp/turn (Baase and Johnson, 1979). An overwinding of the superhelix caused by such a transition will also induce a

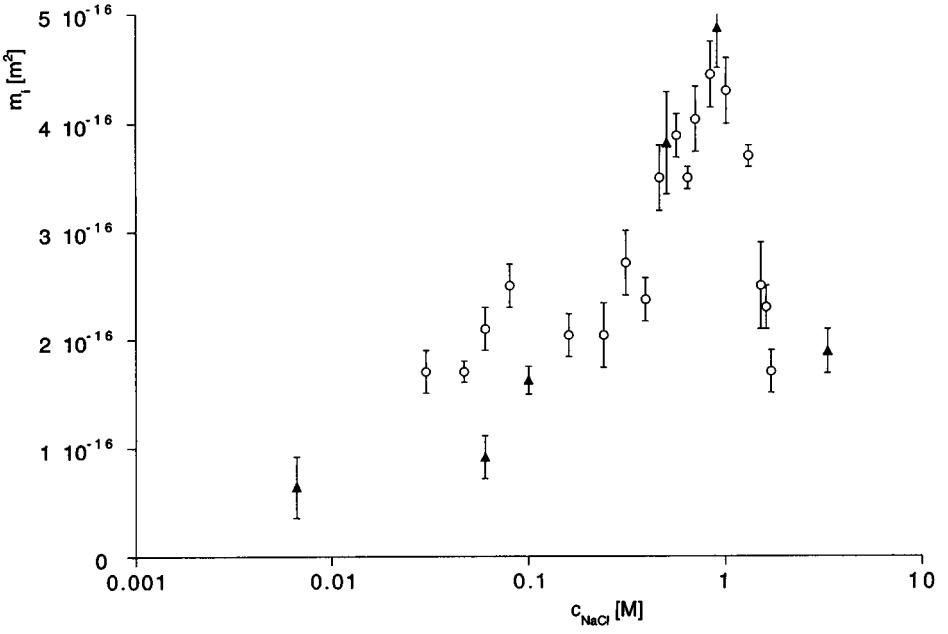

FIGURE 9 The amplitude of the internal relaxation component of the scattered light intensity autocorrelation function increases with the square of the scattering vector. The slope of this increase is plotted as a function of NaCl concentration for p1868 (▲) and SV40 (○).

compaction of the structure, thereby reducing the internal fluctuations. This effect is similar to the known decrease in internal motion with increasing $|\Delta Lk|$, as reported by Klenin et al. (1995).

DNA simulations

Simulations have been performed for p1868 and SV40-DNA as described in Materials and Methods. Starting from a flat circle, the conformation relaxed to a branched interwound structure within 0.3 ms. The SV40-DNA had at least one branch during most of the simulation time, whereas branches in the p1868 conformation occurred only occasionally. This correlated well with the results of Boles et al. (1990), from which almost no branching would be expected for p1686, and a high probability of branching would be expected for SV40.

Fig. 10 shows typical conformations of SV40-DNA after 1 ms of simulation time at different NaCl concentrations. The rows correspond to a NaCl concentration of 10 mM, 100 mM, 500 mM, and 1 M, respectively. The structure

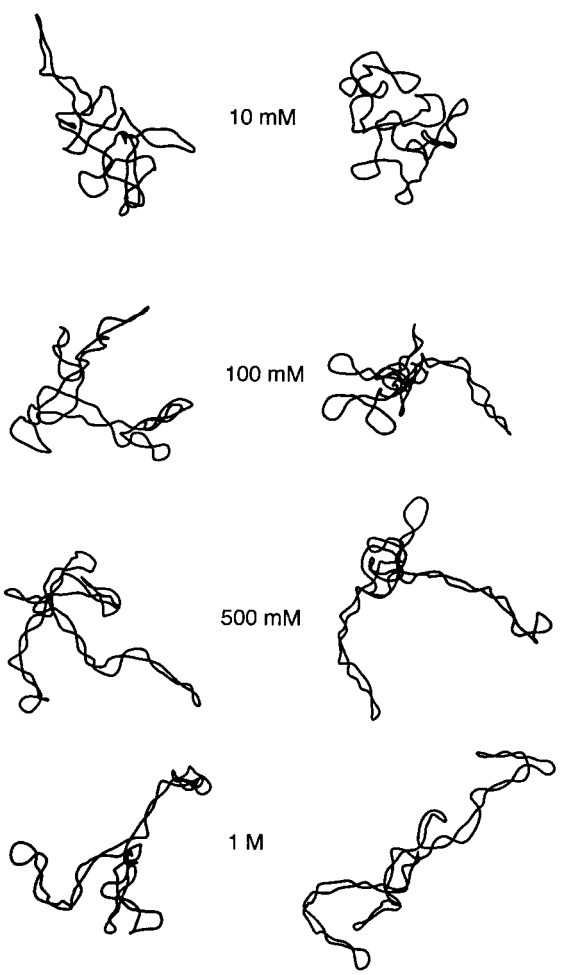

FIGURE 10 Typical conformations of SV40-DNA after 1 ms of simulation time at NaCl concentrations of 10 mM, 100 mM, 500 mM, and 1 M.

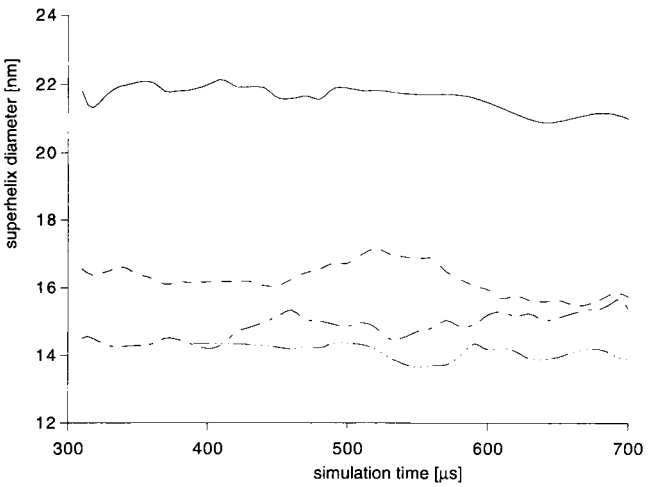

FIGURE 11 Calculated superhelix diameter of SV40-DNA versus simulation time at 10 mM (——), 100 mM (– – –), 500 mM (— - —), and 1 M (— - - - —) NaCl concentrations.

becomes more plectonemic with increasing ionic strength, the strands in the superhelix are closer together at NaCl concentrations above 100 mM. To quantify this phenomenon, we calculated the superhelix diameter as described in Materials and Methods (Eq. 7). The calculated values are plotted versus the simulation time in Fig. 11. A decrease in the superhelix diameter from (22 ± 3) nm at 10 mM NaCl to (14 ± 2) nm at 1 M NaCl concentration confirmed the impression given by the visualized conformations. The superhelix diameter fluctuated by ~0.5 nm in 10 ms; a variation in this fluctuation with ionic strength could not be detected. The radius of gyration (Eq. 4) reached an equilibrium value within ~500 μs (Fig. 12). At 100 mM NaCl ($\delta = 0.008$, $\delta t = 0.1$ ns), we found $R_g = (42.6 \pm 5.0)$ nm for p1868 and $R_g = (74 \pm 5)$ nm for SV40, in good agreement with the measurements (Table 1). Moreover, the behavior of the scattered intensity versus q could be com-

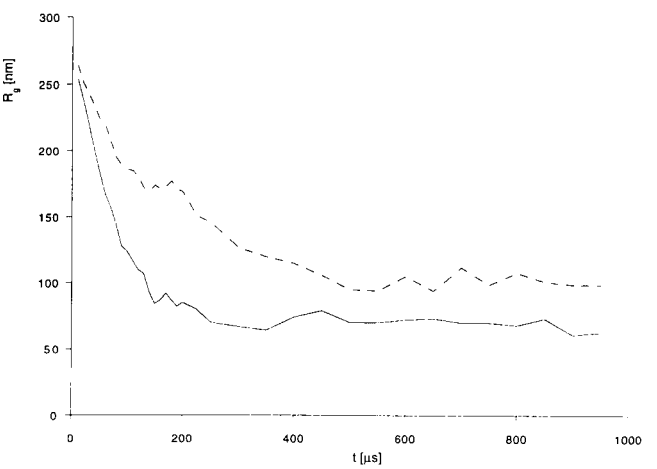

FIGURE 12 BD-simulated radius of gyration of SV40-DNA as a function of simulation time at 0.001 M (– – –) and at 0.1M NaCl concentration (——).

pared directly with the simulated static structure factor $P(q)$ (Eq. 5), averaged over the last 500 μs of the trajectory. The agreement was always satisfactory; a typical comparison is shown in Fig. 13 for SV40 at 100 mM NaCl.

The dynamic structure factor $S(q, \tau)$ was calculated and analyzed for both DNA molecules by using the Fourier decomposition procedure as described in Materials and Methods. We found two components in the ACFs (Eq. 9) with a diffusional behavior: the slope of the corresponding relaxation rates versus q^2 were taken as diffusion coefficients. A comparison of these diffusion coefficients to the experimental findings is shown in Fig. 14 *A* for 100 mM NaCl and in Fig. 14 *B* for 1 M NaCl. The slower component stayed constant, whereas the apparent segmental diffusion coefficient increased at small q^2 because of the q-independent rotational contribution (6Θ; see above). The relative amplitudes $a_2 = A_2/(A_1 + A_2)$ of the simulated internal diffusion coefficients were significantly smaller than the measured ones, but the slope m_i of a linear fit of a_2 versus q^2 (see the section on dynamic light scattering measurements) increased with salt concentration between 1 mM and 1 M NaCl, which was similar to the experiment (Fig. 15). We currently have no good explanation for the discrepancy in the absolute value of the amplitudes; reasons might be the neglect of the anisotropy of the chain segments, or the statistics of the present simulations (see Materials and Methods).

From the good agreement of the static and dynamic structure factors with the experimental values (except for the amplitudes of the internal relaxation), we conclude that BD simulations are a useful tool for understanding the mechanism of DNA supercoiling and the influence of cations on the structure and dynamics of the DNA. The measured increase of the segmental motions with increasing NaCl concentration could be observed qualitatively in the simulations. Furthermore, the simulated radius of gyration of p1868 decreased monotonically with the ionic strength (data not shown). Because an increase of the ion concentration is taken into account by a decrease in the Debye length in the simulations, the compaction of the DNA with increasing NaCl concentration seems to be due to the screening of the phosphate backbone, as supposed above.

CONCLUSIONS

We have studied salt effects on the structure and internal dynamics of two superhelical DNAs: p1868, a bacterial plasmid of 1868 base pairs, and SV40, a eukaryotic viral DNA of 5243 base pairs. The static light scattering measurements suggest a salt-dependent DNA compaction, especially above 1 M, which may be due to DNA branching, as indicated by lower values of the radius of gyration and by a reduction of the measured end-to-end distances of an equivalent Gaussian chain. Dynamic light scattering experiments indicate that the translational diffusional coefficient is not significantly affected by NaCl concentration. The internal motions of the superhelix manifest themselves in a fast-relaxing component in the light scattering autocorrelation function (ACF), which can be characterized by an internal diffusion coefficient at high scattering vectors, and by its amplitude relative to the slow relaxation due to translational motion. Whereas the internal diffusion coefficient does not change with NaCl concentration, the amplitude of the segmental motions changes significantly, with a maximum at ~1 M for both DNA molecules. We tentatively interpret this effect to be caused by a competition between increasing electrostatic screening of the negatively charged phosphate backbone of the DNA by the Na^+ counterions, which allows wider intramolecular motions, and DNA compaction, which hinders them. Similar to the recent findings of Gebe et al. (1996), a lateral collapse of the interwound structure for Na^+ concentrations greater than 0.1 M, as observed by Bednar et al. (1994) in cryoelectron micros-

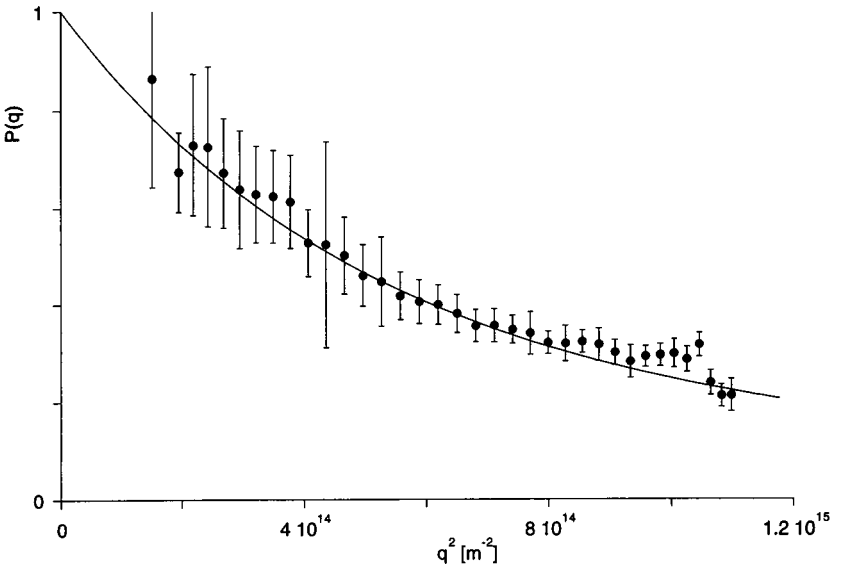

FIGURE 13 Comparison of the measured (●) and BD-simulated (——) static structure factor of SV40-DNA at 100 mM NaCl concentration.

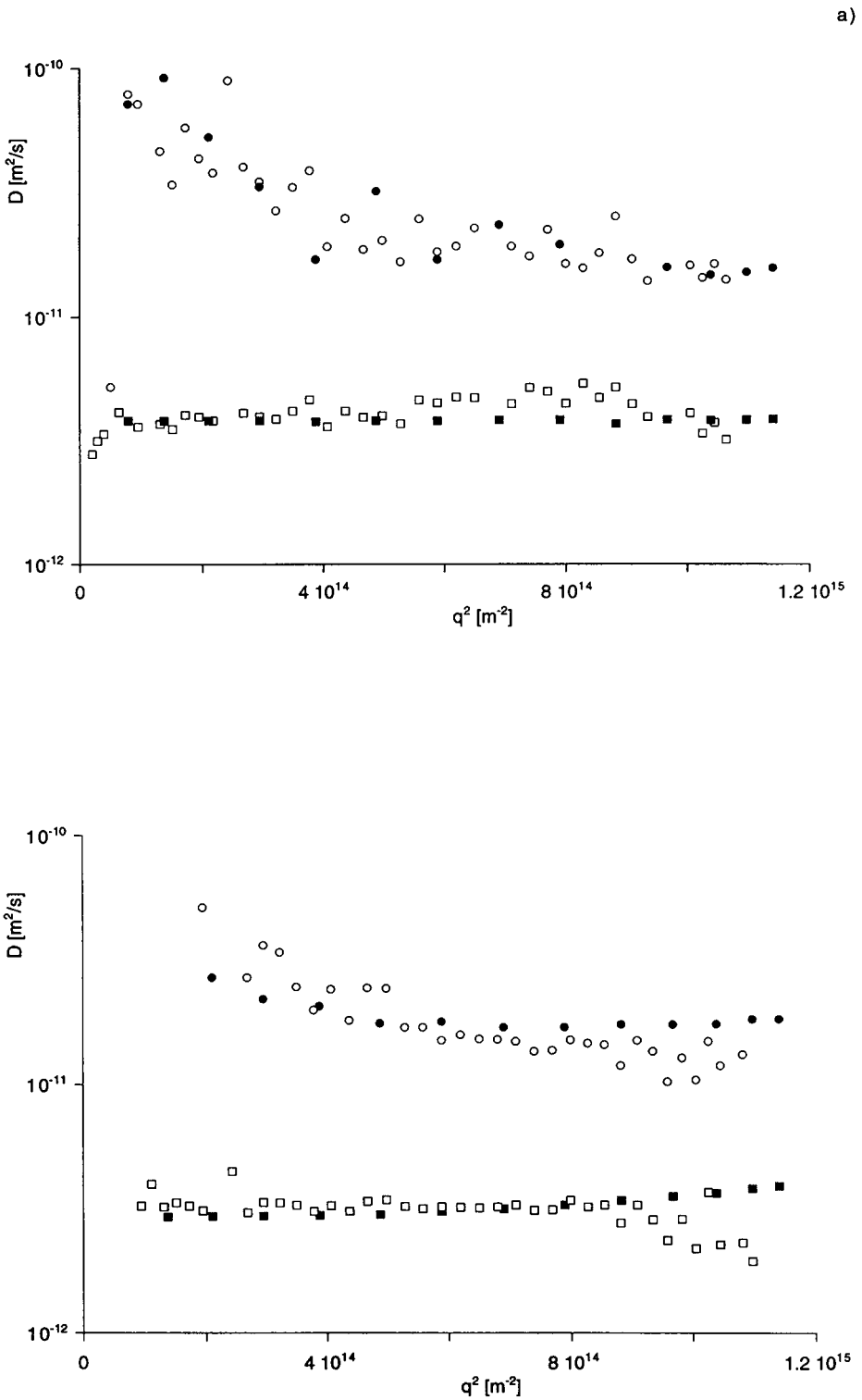

FIGURE 14 (*A*) Measured (□, ○) and simulated (■, ●) diffusion coefficients of SV40-DNA at 0.1 M NaCl concentration. The segmental diffusion coefficient (○, ●) increases at small q^2 because of end-over-end rotational motion of the molecule. (*B*) Measured (□, ○) and simulated (■, ●) diffusion coefficients of SV40-DNA at 1.0 M NaCl concentration.

copy studies, is not supported by our data for superhelical DNA in free solution.

The experimental data can be very well reproduced by Brownian dynamics simulations, which yield static structure factors and translational diffusion coefficients in good agreement with the experiments. The superhelix diameter decreases with increasing ionic strength from (22 ± 3) nm at 10 mM NaCl to (14 ± 2) nm at 1 M NaCl concentration. By using a Fourier decomposition procedure, it has been possible to compute the segmental motion part of the dynamic structure factor on the simulated trajectories. The segmental motion amplitudes of the simulated ACFs increase with salt concentration in a manner similar to that of the measured ones up to 1 M NaCl.

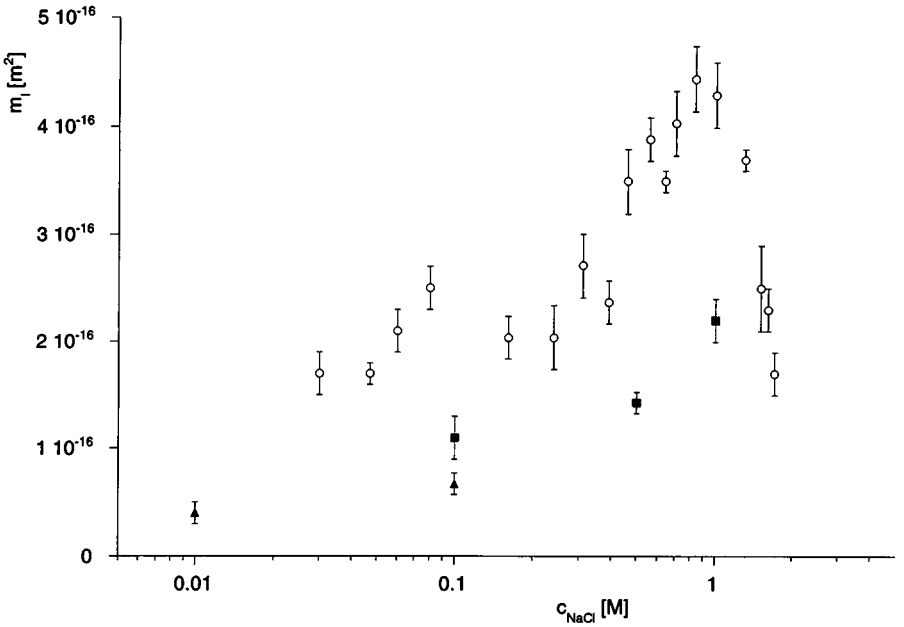

FIGURE 15 Slope of the q^2-dependent increase in the relative amplitude of the internal relaxation component of SV40-DNA as a function of NaCl concentration. ○, Measured data. ■, Simulation, $\delta = 0.08$, $\delta t = 1$ ns. ▲, Simulation, $\delta = 0.008$, $\delta t = 0.1$ ns.

The increase of the segmental motions with cation concentration might not only be caused by a change in the cation concentration of the bulk solution; it might also be a local effect, caused, for example, by screening of the phosphate charges by a bound protein. Studies of the influence of divalent cations or combinations of different cations on the internal dynamics of the DNA under near-in vivo conditions might be helpful in elucidating such effects.

We thank Konstantin Klenin and Gero Wedemann for help with the programs and Nathalie Brun and Gabriele Müller for assistance with DNA preparations. Thanks are also due to Katalin Tóth and Karsten Rippe for critical reading of the manuscript.

Parts of this work were supported by BMBF grant 01KW9620 to JL and NATO collaborative research grant CRG910239 to JL and GC.

REFERENCES

Anderson, P., and W. Bauer. 1978. Supercoiling of closed circular DNA: dependence upon ion type and concentration. *Biochemistry.* 17: 594–601.

Baase, W. A., and W. C. J. Johnson. 1979. Circular dichroism and DNA secondary structure. *Nucleic Acids Res.* 6:797–814.

Bednar, J., P. Furrer, A. Stasiak, J. Dubochet, E. H. Egelman, and A. D. Bates. 1994. The twist, writhe and overall shape of superhelical DNA change during counterion-induced transition from a loosely to a tightly interwound superhelix. Possible implications for DNA structure in vivo. *J. Mol. Biol.* 235:825–847.

Berg, O. G. 1979. Dynamics of circular wormlike chains. *Biopolymers.* 18:2861–2874.

Boles, T. C., J. H. White, and N. R. Cozzarelli. 1990. Structure of plectonemically supercoiled DNA. *J. Mol. Biol.* 213:931–951.

Borowiec, J. A., L. Zhang, S. Sasse-Dwight, and J. D. Gralla. 1987. DNA supercoiling promotes formation of a bent repression loop in lac DNA. *J. Mol. Biol.* 196:101–111.

Chirico, G., and J. Langowski. 1992. Calculating hydrodynamic properties of DNA through a second-order Brownian dynamics algorithm. *Macromolecules.* 25:769–775.

Chirico, G., and J. Langowski. 1994. Kinetics of DNA supercoiling studied by Brownian dynamics simulation. *Biopolymers.* 34:415–433.

Chirico, G., and J. Langowski. 1996. Brownian dynamics simulations of supercoiled DNA with bent sequences. *Biophys. J.* 71:955–971.

Doi, M., and S. F. Edwards. 1986. The Theory of Polymer Dynamics. Oxford University Press, Oxford.

Gebe, J. A., J. J. Delrow, P. J. Heath, B. S. Fujimoto, D. W. Stewart, and J. M. Schurr. 1996. Effects of Na^+ and Mg^{2+} on the structures of supercoiled DNAs: comparison of simulations with experiments. *J. Mol. Biol.* 262:105–128.

Gebe, J. A., and J. M. Schurr. 1993. Intramolecular interference effects in dynamic light-scattering from rigid rings. *Biopolymers.* 33:1757–1764.

Gull, S. F., and G. J. Daniell. 1978. Image reconstruction from incomplete and noisy data. *Nature.* 272:686–690.

Hagerman, P. J. 1988. Flexibility of DNA. *Annu. Rev. Biophys. Biophys. Chem.* 17:265–286.

Kapp, U., and J. Langowski. 1992. Preparation of DNA topoisomers by RP-18 high performance liquid chromatography. *Anal. Biochem.* 206: 293–299.

Klenin, K., M. D. Frank-Kamenetskii, and J. Langowski. 1995. Modulation of intramolecular interactions in superhelical DNA by curved sequences. A Monte Carlo simulation study. *Biophys. J.* 68:81–88.

Kratky, O., and G. Porod. 1949. Röntgenuntersuchung gelöster Fadenmoleküle. *Rec. Trav. Chim.* 68:1106–1113.

Kremer, W., K. Klenin, S. Diekmann, and J. Langowski. 1993. DNA curvature influences the internal motion of superhelical DNA. *EMBO J.* 12:4407–4412.

Langowski, J. 1987. Salt effects on internal motions of superhelical and linear pUC8 DNA. *Biophys. Chem.* 27:263–271.

Langowski, J. 1997. Modelling large DNA molecules: long-range interactions and regulation of transcription. *In* Nucleic Acids and Molecular Biology. Springer, Heidelberg.

Langowski, J., and R. Bryan. 1991. Maximum entropy analysis of photon correlation spectroscopy data using a Bayesian estimate for the regularization parameter. *Macromolecules.* 24:6346–6348.

Langowski, J., G. Chirico, and U. Kapp. 1994a. DNA supercoil dynamics studied by dynamic light scattering and Brownian dynamics simulations. *In* Structural Biology: The State of the Art. Adenine Press, Schenectady, NY. 175–189.

Langowski, J., and U. Giesen. 1989. Configurational and dynamic properties of different length superhelical DNAs measured by dynamic light scattering. *Biophys. Chem.* 34:9–18.

Langowski, J., U. Giesen, and C. Lehmann. 1986. Dynamics of superhelical DNA studied by photon correlation spectroscopy. *Biophys. Chem.* 25:191–200.

Langowski, J., U. Kapp, K. Klenin, and A. Vologodskii. 1994b. Solution structure and dynamics of DNA topoisomers. Dynamic light scattering studies and Monte Carlo simulations. *Biopolymers.* 34:639–646.

Langowski, J., W. K. Olson, S. C. Pedersen, I. Tobias, T. P. Westcott, and Y. Yang. 1996. DNA supercoiling, localized bending and thermal fluctuations. *Trends Biochem. Sci.* 21:50.

Laundon, C. H., and J. D. Griffith. 1988. Curved helix segments can uniquely orient the topology of supertwisted DNA. *Cell.* 52:545–549.

Lewis, R., J. H. Huang, and P. Pecora. 1985. Rotational and translational motion of supercoiled plasmids in solution. *Macromolecules.* 18: 944–948.

Provencher, S. 1984. CONTIN V2 User's Manual, EMBL Technical Report. European Molecular Biology Laboratory, Heidelberg, Germany.

Richter, G. 1997. Elektrostatische Effekte auf die Struktur superhelikaler DNA. Diplomarbeit Fachbereich Chemie. Universität Hannover, Hannover, Germany.

Schurr, J. M. 1977. Theory of dynamic light scattering by polymers and gels. *Chem. Phys.* 30:243–247.

Skilling, J., and R. K. Bryan. 1984. Maximum entropy image reconstruction: general algorithm. *Mon. Not. R. Astr. Soc.* 211:111–124.

Soda, K. 1984. Theory of the dynamic light scattering properties for circular semiflexible chains in solution. *Macromolecules.* 17: 2365–2375.

Stigter, D. 1977. Interactions of highly charged colloidal cylinders with applications to double stranded DNA. *Biopolymers.* 16:1435–1448.

ten Heggeler-Bordier, B., W. Wahli, M. Adrian, A. Stasiak, and J. Dubochet. 1992. The apical localization of transcribing RNA polymerases on supercoiled DNA prevents their rotation around the template. *EMBO J.* 11:667–672.

Vologodskii, A. V., S. D. Levene, K. V. Klenin, M. D. Frank-Kamenetskii, and N. R. Cozzarelli. 1992. Conformational and thermodynamic properties of supercoiled DNA. *J. Mol. Biol.* 227:1224–1243.

Waldeck, W., H. Zentgraf, and F. Rösl. 1988. Topoisomerase II inhibitors influence simian virus 40 chromatin structure in vivo accompanied with inhibition of replication, transcription and changes in DNA supercoiling. *Oncology.* 45:107–116.

Zhang, P. S., I. Tobias, and W. K. Olson. 1994. Computer simulation of protein-induced structural changes in closed circular DNA. *J. Mol. Biol.* 242:271–290.